


## PAPER

[View Article Online](#)  
[View Journal](#) | [View Issue](#)

Cite this: *Polym. Chem.*, 2024, **15**, 2318

# Bridging of poly(acetylene)s and PEG-modified poly(olefin)s through ring-opening metathesis copolymerization (ROMCP)<sup>†</sup>

Santhosh Kumar Podiyanachari,<sup>a</sup> Maciej Bartóg,<sup>b</sup> Mohammed Al-Hashimi <sup>\*b</sup> and Hassan S. Bazzi <sup>\*a,c</sup>

Amphiphilic copolymers of highly conjugated poly(acetylene)s and poly(ethylene glycol)-functionalized perylene diimide (PEG<sub>750</sub>–PDI)-incorporating poly(olefin)s have been synthesized *via* tandem cyclopolymerization and ring-opening metathesis copolymerization (ROMCP) methodologies. Both di- and tri-block copolymers were prepared from 1,6-heptadiyne and oxanorbornene imide-based cycloolefin monomers using ruthenium-based alkylidene initiators. The relative atomic weight percentages of both di- and tri-block copolymers were estimated using X-ray photoelectron spectroscopy (XPS) analysis. Photophysical properties of both copolymers have been explained based on both UV-Vis and fluorescence spectroscopic analysis shedding more light on their different stages of organization as well as the  $\pi$ – $\pi$  stacking interactions of the PEG<sub>750</sub>–incorporating perylene cores in aqueous solutions. Furthermore, these investigations elucidate the modulation of the photophysical properties and H-type aggregation processes of polymers in aqueous solutions that lead to the formation of PEG<sub>750</sub>–PDI-derived amphiphiles. Copolymeric surface analysis, segmental patterns and film morphology were examined by atomic force microscopy (AFM) revealing globular or spherical morphological features enhanced by various functional groups present in the polymer bulk. In addition, the formation of these spherical morphologies was further visualized in the thin film cross-sections of both di- and tri-block polymers by scanning electron microscopy (SEM) to confirm the surface morphologies determined by AFM analysis of both polymeric materials.

Received 21st January 2024,

Accepted 9th May 2024

DOI: 10.1039/d4py00078a

[rsc.li/polymers](https://rsc.li/polymers)

## Introduction

Metathesis polymerization is a well-established technique used for synthesizing conjugated poly(acetylene)s and poly(ene)s from terminal dialkyne monomers.<sup>1,2</sup> Conjugated poly(acetylene)s acquired through cyclopolymerization of functionalized 1,6-heptadiyne monomers using metathesis catalysts exhibit cyclic structures along the conjugated backbone, particularly those derived from oxidative polymerization. This unique structural feature provides enhanced stability and excellent processability of the resulting polymers.<sup>3,4</sup> The repeat units of these polymers can consist of either five-membered rings (*via*  $\alpha$ -addition) or six-membered rings (*via*  $\beta$ -addition),

or a combination of both, depending on the alkyne unit's insertion mode into the metal–alkylidene initiator.<sup>1,2</sup> This versatility in ring formation imparts a tailored and tunable aspect to the resulting polymer structure, enabling fine control over its properties. Among various catalytic systems, Schrock and Buchmeiser reported pioneering results in the cyclopolymerization of various terminal dialkynes, such as 1,6-heptadiynes, using well-defined [Mo]- or [Ru]-based metathesis initiators.<sup>2,3,5–7</sup> Later, many cyclopolymerization-derived conjugated poly(acetylene)s were synthesized and have been well utilised for various conducting applications.<sup>8–11</sup>

Choi and co-workers also explored different Grubbs' catalysts for the cyclopolymerization of different functionalized terminal di(alkyne) monomers. Their investigation led to the synthesis of the first example of  $\beta$ -selective cyclopolymerization-derived poly(ene)s, characterized by exclusive incorporation of six-membered ring structures along the polymer backbone.<sup>12–20</sup> Those conjugated polymers obtained *via* cyclopolymerization have found extensive use in the fabrication of nanosheets, nanoparticles, and various self-assembly applications.<sup>21–26</sup> Furthermore, Choi has extended the application of cyclopolymerization, by reporting the synthesis of

<sup>a</sup>Division of Arts and Science, Texas A&M University at Qatar, P.O. Box 23874, Doha, Qatar. E-mail: [hassan.bazzi@qatar.tamu.edu](mailto:hassan.bazzi@qatar.tamu.edu)

<sup>b</sup>Department of Chemical Engineering, Texas A&M University at Qatar, P.O. Box 23874, Doha, Qatar. E-mail: [mohammed.al-hashimi@qatar.tamu.edu](mailto:mohammed.al-hashimi@qatar.tamu.edu)

<sup>c</sup>Department of Materials Science & Engineering, Texas A&M University, 209 Reed MacDonald Building, College Station, TX 77843-3003, USA

<sup>†</sup>Electronic supplementary information (ESI) available. See DOI: <https://doi.org/10.1039/d4py00078a>



diblock copolymers, combining cyclopolymerization with ring-opening metathesis (ROM). Copolymers obtained *via* cyclopolymerization and ROMCP have been specifically employed in the preparation of nanostructures and the synthesis of poly(olefin)-linked conjugated poly(ene)s under controlled and living polymerization.<sup>16,27–29</sup> In addition, such random and diblock copolymers containing conjugated polymer backbones with various functionalities have been well-studied in various self-assembly applications.<sup>30</sup>

However, there are a limited number of reports on the synthesis of such copolymers based on poly(ene)s and poly(olefin)s *via* tandem cyclopolymerization and ROMCP in a unified, one-step metathesis polymerization process. Our research group has actively contributed to this field, investigating the alkyne-insertion metathesis polymerization<sup>31</sup> and ROMP reactivities of diverse functional and nonfunctional cycloolefin monomers using Grubbs or Hoveyda–Grubbs type [Ru]–alkylidene initiators. This approach has led to the development of a new class of structurally well-defined poly(olefin)s.<sup>32–37</sup> Our efforts have yielded a series of functional poly(olefin)s based on polypentenamers,<sup>36,38</sup> poly(vinyl alcohol)s,<sup>34,38</sup> poly(norbornene)s<sup>32,33,39,40</sup> and rhodamine-based poly(olefin)s showcasing versatility in material design for various biological applications.<sup>41,42</sup> We recently reported the synthesis of highly conjugated *bay*-functional perylene diimide chromophore incorporating poly(oxanorbornene imide)s *via* ROMP,<sup>43</sup> by investigating their hyperbranched propensity behavior.<sup>44</sup> Based upon our findings, ROMP-derived poly(olefin)s containing PDI-grafted alkoxy-functionalized poly(oxanorbornene imide)s are promising candidates for the preparation of a diverse range of novel polymeric materials tailored for applications in organic electronics.<sup>43,44</sup>

In this work, we describe a tandem approach for the synthesis of amphiphilic copolymers, combining conjugated poly(acetylene)s and poly(ethylene glycol)-incorporating perylene diimide (PEG<sub>750</sub>–PDI)-grafted poly(olefin)s *via* cyclopolymerization and ROMCP. The copolymers derived from PEG–PDI have attracted considerable attention, particularly due to their unique structural and dynamic characteristics in diluted aqueous solutions.<sup>45–49</sup> Investigations by various research groups have revealed the amphiphilic nature of these compounds and their self-assembly behavior, driven by a delicate interplay between hydrophobic and  $\pi$ – $\pi$  interactions. The capacity to manipulate their aggregation behavior through molecular engineering, temperature variation, and solvent composition has paved the way for the incorporation of these systems into a diverse range of applications, including catalysis, membranes, nanotubes, sensing and bioimaging agents.<sup>50–54</sup> Furthermore, the photoluminescence properties of this class of materials, such as the quantum yield ( $\phi_{\text{PL}}$ ) of PDI derivatives, often face limitations, like aggregation caused quenching (ACQ) at high concentration in solution or in the solid film state. Tuning the fluorescent properties of the PDI unit from ACQ to aggregation induced emission (AIE) has been typically achieved *via* molecular engineering of both the amide and *bay* functionality with bulky groups designed to

control the  $\pi$ – $\pi$  stacking and aggregation behavior.<sup>55–57</sup> Our tandem approach offers a versatile platform for accessing a range of tunable PEG<sub>750</sub>-incorporating chromophores within the non-conjugated polymer matrix, serving as a copolymer counterpart of the cyclopolymerization-derived conjugated poly(acetylene). Our findings demonstrate that tandem cyclopolymerization, followed by ROMP, yields copolymers with diverse properties and applications including electrical conductivity, bioimaging and photoluminescence. This methodology provides a promising route for the preparation of novel polymeric materials with tailored properties.

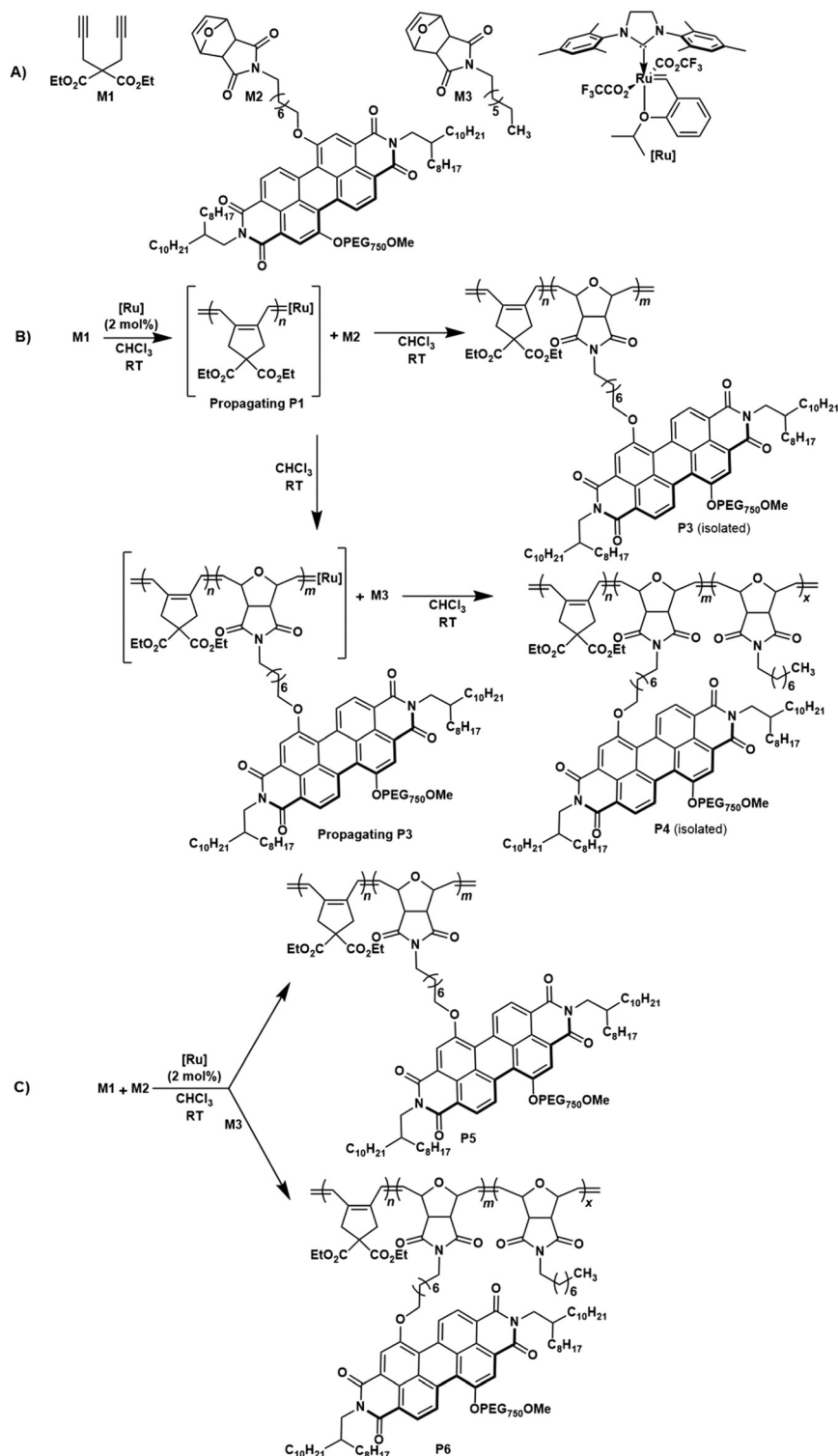
To the best of our knowledge, this work constitutes the first example of incorporating perylene cores into a non-conjugated polymer, with optical properties modulated by the poly(ene) block composition and the polarity of the medium. This innovative approach to control PDI aggregation through the strategic integration of perylene cores into non-conjugated polymers, coupled with the tunable and reversible nature of the interactions, introduces new avenues for the advancement of this class of systems. The modular composition of the copolymer, allowing for tailored adjustments, presents a versatile platform with potential applications across various fields.

## Results and discussion

### Polymer synthesis

The molecular structures of all the monomers (**M1**–**M3**) and the ruthenium–alkylidene initiator [Ru] are outlined in Scheme 1A. The dialkyne-terminal monomer dipropargyl diethyl malonate (DEDPM) **M1** was synthesized following a previously reported method.<sup>58</sup> The cycloolefin monomers PEG<sub>750</sub>–PDI-based oxanorbornene imide monomer **M2**<sup>59,60</sup> (Fig. S1 and S2, ESI†) and *N*-alkyl substituted oxa-norbornene imide monomer **M3**<sup>61</sup> were synthesized following a modified procedure based on prior reports.<sup>59</sup> Poly(acetylene) **P1** was derived from cyclopolymerization of 1,6-hexadiyne **M1** using a trifluoroacetate modified Hoveyda–Grubbs type 2<sup>nd</sup> generation catalyst,<sup>62</sup> resulting in polymer **P1** as a dark-red solid.<sup>62</sup> Additionally, PDI-based oxa-norbornene imide **M2** underwent polymerization using the same initiator, yielding the ROMP-derived **P2** as a dark red solid. To extend the cyclopolymerization by incorporating both hydrophilic and hydrophobic units into the polymers, diblock copolymer **P3** was synthesized *via* cyclopolymerization of **M1**, followed by the addition of PEG<sub>750</sub>-derived PDI oxa-norbornene imide monomer **M2** *via* ROMCP. Copolymerization was carried out with a 1:1 ratio of both monomers using a 2 mol% catalyst loading, and the monomer conversion was monitored by <sup>1</sup>H NMR spectroscopy. After terminating the polymerization using ethyl vinyl ether, the resulting polymer was purified *via* precipitation of the concentrated polymer solution in *n*-pentane. After multiple reprecipitations, the pure copolymer **P3** was isolated as a dark-red solid in excellent yield (98%) (Scheme 1B). Similarly, triblock copolymer **P4** was synthesized in a 1:1:1 ratio *via* cyclopolymerization with **M1**, followed by ROMCPs of **M2** and **M3** to yield a dark-red





**Scheme 1** (A) Structure of monomers **M1**–**M3** and trifluoroacetate-modified Hoveyda–Grubbs type 2<sup>nd</sup> generation catalyst **[Ru]**, (B) synthesis of diblock copolymer **P3**, and triblock copolymer **P4**, (C) synthesis of random binary copolymer **P5** and ternary copolymer **P6**.

solid in excellent yield (96%) (Scheme 1B). In addition, random versions of diblock polymer **P5** and triblock polymer **P6** were synthesized using the same monomer ratio and catalyst loading (Scheme 1C). Both **P5** and **P6** were isolated as dark

red solids in excellent yields (95% isolated yield for **P5** and 97% for **P6**).

The copolymer composition and structural features of copolymers **P3**–**P6** were characterized by <sup>1</sup>H NMR spectroscopy. The



$^1\text{H}$  NMR spectrum of copolymer **P3** displays a broad multiplet together with a singlet signal ranging from  $\delta = 6.6$ – $6.9$  ppm, indicating olefinic protons within the conjugated backbone of poly(acetylene) (**P1**), resulting from the cyclopolymerization of the dialkyne monomer **M1** and the olefinic protons of the poly(oxanorbornene imide) copolymer counterpart derived from PEG-containing oxanorbornene imide monomer **M2**. Triblock copolymer **P4** shows an additional olefinic proton signal along with the abovementioned peaks for **P3** as a broad singlet signal at 6.0 ppm representing the poly(oxanorbornene imide) copolymer counterpart derived from *N*-alkyl substituted oxanorbornene imide monomer **M3** (Fig. S3–S6, ESI†). In the  $^1\text{H}$  NMR spectra of random diblock **P5** and triblock **P6** copolymers, olefinic proton signals appeared as heterodyad peaks around 6.9 ppm and 5.9 ppm indicating olefinic proton signals of conjugated backbones and poly(oxanorbornene imide)s (Fig. S7–S10, ESI†).

The relative atomic weight percentages of the constituent elements in copolymers **P3** and **P4** were further characterized by XPS analysis. In the XPS spectra, characteristic signals corresponding to carbon, nitrogen and oxygen atoms within the copolymer composition were observed, with corresponding binding energies (BE) at 282 eV for carbon, 397 eV for nitrogen, and 529 eV for oxygen, respectively (Fig. S11†). These binding energy values were consistent for carbon, nitrogen, and oxygen in both diblock **P3** and triblock **P4** polymers. The relative atomic weight percentages estimated from the peak areas of the carbon, nitrogen and oxygen signals were determined for diblock copolymer **P3** as 74.79% for carbon, 1.19% for nitrogen, and 20.68% for oxygen. In the case of the triblock copolymer **P4**, the relative atomic weight percentages were estimated as 77.33%, 1.99%, and 24.02%, respectively, for carbon, nitrogen, and oxygen. The slight excess in the relative weight percentages of carbon, nitrogen, and oxygen in the case of the triblock copolymer further indicates the presence of different C, N, and O proportions in the triblock copolymer **P4**. This XPS analysis provides additional confirmation of the distinct atomic weight percentages of the di- and tri-block copolymers.

### Molecular weights and thermal stability of the polymers

The number average molecular weights ( $M_n$ ) of the polymers **P3**–**P6** were measured using size-exclusion chromatography (SEC) in chlorobenzene. By SEC analysis, we aimed to investigate  $M_n$  as well as the amount of diblock and triblock copolymers obtained *via* tandem metathesis polymerization. The obtained copolymers displayed relatively high molecular weights with slightly elevated dispersities ( $D$ ), *i.e.*,  $M_n = 62.0$  kDa with  $D$  of 1.5 for **P3**,  $M_n = 79.0$  kDa with  $D$  of 2.1 for **P4**,  $M_n = 74.3$  kDa with  $D$  of 1.9 for **P5** and  $M_n = 88.3$  kDa with  $D$  of 2.4 for **P6** (Fig. S12, ESI†). These high  $M_n$  values demonstrate the formation of copolymers *via* combining both conjugated poly(acetylene) backbones and poly(olefin)s in the case of both di- and tri-block polymers. The SEC traces of the polymers displayed a slightly bimodal distribution, and this is possibly due to partial catalyst deactivation that should lead to copolymer randomization during the formation of the di- and

tri-block polymers. However, the larger values of  $D$  observed for these polymers can be attributed to chain coupling, leading to the formation of significant chain transfer during the secondary metathesis polymerization.<sup>63,64</sup> These results contribute to a comprehensive understanding of the structural characteristics and macromolecular compositions of the synthesized copolymers.

The stability of copolymers **P3** and **P4** was investigated by thermal gravimetric analysis (TGA), conducted in a temperature range from 30 to 800 °C at a heating rate of 10 °C min<sup>−1</sup> under a nitrogen atmosphere. The thermal decomposition temperatures ( $T_d$ ) corresponding to 5% weight loss were determined, resulting in  $T_d$  values of 219 °C and 377 °C for **P3**, and 234 °C, 391 °C, 484 °C for **P4** (Fig. S13, ESI†). The high thermal degradation temperature for diblock copolymer **P3** can be attributed to the presence of the conjugated poly(ene) in the main chain and the incorporation of the bulky PEG<sub>750</sub>–PDI-based cycloolefin as the copolymeric counterpart. Similarly, **P4** containing a bulky polyolefinic counterpart of PEG<sub>750</sub>–PDI and alkyl-functionalized oxanorbornene imide units along with the conjugated poly(acetylene) led to the three different degradation temperatures mentioned above. These molecular and structural features play an important role in enhancing the thermal stability of the copolymers. Differential scanning calorimetry (DSC) was used to determine the glass transition temperature ( $T_g$ ). The samples were initially heated from 30 to 400 °C to complete the first cycle of the calorimetry experiment, then cooled to room temperature, and re-heated again from 30 to 400 °C at a heating/cooling rate of 10 °C min<sup>−1</sup>. There was no significant  $T_g$  value recorded for the copolymer samples in the temperature range from 40 to 400 °C. This absence of a glass transition temperature aligns with observations in previously reported PDI-derived polymers.<sup>44,59</sup>

### Photophysical properties

In order to study changes in the aggregation modes across the series of copolymers, full photophysical characterization was performed. As depicted in Fig. 1a, the UV-Vis spectra of PEG<sub>750</sub>–PDI-derived random copolymers **P5** and **P6**, recorded in chloroform, display characteristic perylene  $S_{0-0}$  transition signals around 573 nm and  $S_{0-1}$  dependent maxima at 534 nm as well as a low intensity  $S_{0-2}$  signal at 400 nm. The first absorption band in this range is commonly referred to as the “fingerprint” region for PDI derivatives, and it highly depends on the presence of  $\pi$ – $\pi$  interactions between perylene cores.<sup>65</sup> Both absorption maxima are significantly red-shifted compared to the unsubstituted PDI moiety.<sup>66</sup> This shift is attributed to the presence of electron-donating substituents in the *bay* position, which expands the system's conjugation, and therefore narrows the band gap.<sup>67–70</sup> The absorption profiles of the PEG<sub>750</sub>–PDI-derived copolymers **P5** and **P6** (Fig. 1a) in solution are virtually identical and display similar spectroscopic changes when measured in the thin film state (Fig. 1a). The films of copolymers **P5** and **P6** show a clear blueshift of the absorption to 513 nm with complete disappearance of the





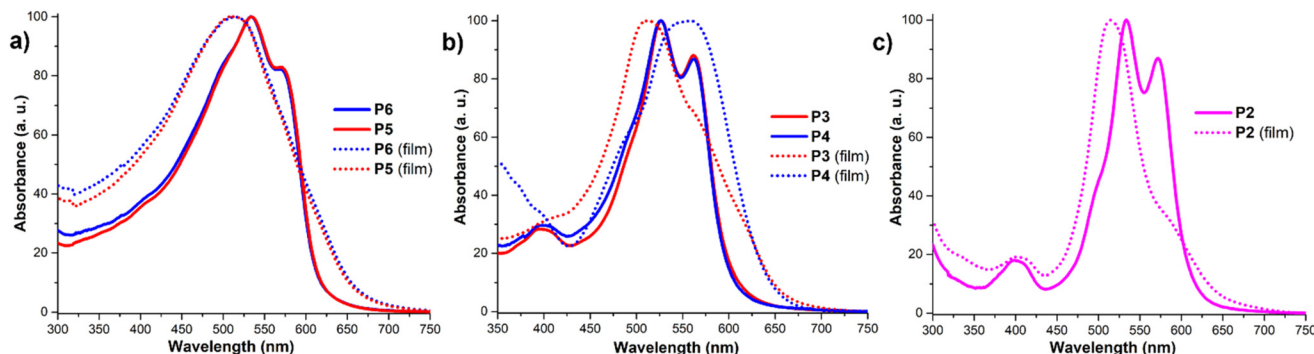


**Fig. 1** UV-Vis absorption spectra of (a) random binary **P5** and ternary **P6** copolymers, (b) diblock **P3** and triblock **P4** copolymers, and (c) PEG<sub>750</sub>-PDI-derived homopolymer **P2** in chloroform (solid lines) and their thin film state cast from the same solvent (dotted lines).

secondary peak. This indicates the presence of strong  $\pi$ - $\pi$  interactions accompanied by the formation of H-aggregates of the PDI moieties.<sup>71,72</sup> For the random copolymers **P5** and **P6**, the absorption profiles depend on the average interactions between perylene cores, while polyacetylene does not show interference in the absorption profile.

The UV-Vis absorption spectra of the tandem cyclopolymerization- and ROMP-derived block copolymers are displayed in Fig. 1b and c revealing specific characteristic features. In solution polymers **P2**, **P3** and **P4** show virtually identical profiles with a characteristic double maximum at 527 and 563 nm. Additionally, all 3 polymer solutions exhibit a shoulder around 500 nm, which was assigned to the presence of the polyacetylene fragment with high absorption in this region.<sup>6</sup> In the solid film state, polymers **P2**, **P3**, and **P4** exhibit substantially different absorption profiles, despite no changes to the chromophore core. Polymer **P2** in the solid film exhibits an almost complete absence of the  $S_{0-0}$  transition signal and a significant blueshift of the  $S_{0-1}$  maxima to 514 nm. This phenomenon was attributed to strong  $\pi$ - $\pi$  interactions between perylene cores, further supported by regular distances between them, enforced by the homopolymeric structure of the backbone. The film of the diblock polymer **P3** shows an absorption profile like that of polymer **P2** with a single absorption peak blue shifted to 512 nm indicating similar  $\pi$ - $\pi$  interactions and formation of H-aggregates. On the other hand, the triblock polymer **P4** exhibits its maximum absorption red-shifted to 556 nm as a broad band with a shoulder around 500 nm. These differences underscore the significant variations in perylene aggregation behavior influenced by the polymer structure. We assume that changes in the stacking of the perylene cores and thus changes in the absorption spectra are the result of the interplay of several factors such as  $\pi$ - $\pi$  stacking and hydrophilic and lipophilic fragment interactions combined with steric effects exerted by the polymer backbone. Moreover, the reduction of the intensity of the 0-0 and 0-1 absorption peaks and the drop in fluorescence efficiency indicate H-type aggregation rather than J-type aggregation in the THF and THF/water solutions.<sup>73</sup>

The modular structure of block copolymers **P3** and **P4** allows for the introduction of both hydrophobic hydrocarbon and aromatic groups, as well as hydrophilic PEG<sub>750</sub>. This composition enables precise control of the polymer aggregation based on the medium's polarity. The amphiphilic nature of these PEG<sub>750</sub>-PDI-based polymers allows them to be dissolved in typical hydrophobic solvents like chloroform or chlorobenzene, as well as highly polar solvents such as DMF and methanol, which has been also reported for other PDI derivatives.<sup>74</sup> These features allow amphiphiles to self-assemble in aqueous solutions making them suitable for use as markers in biological systems.<sup>54</sup> This self-assembly behaviour results in significant changes in both their absorption and emission spectra, which are influenced by the polymer composition and polarity of the solvent. The absorption profile in THF/water solutions shows a decrease in the intensity of the vibronic progression peak around 530 nm, illustrating the effect of the aqueous fraction on the aggregation behaviour of the polymers (Fig. 2a-c).

This effect has been widely reported in the literature and is typically assigned to the formation of aggregates with strong  $\pi$ - $\pi$  stacking interactions among the PDI cores in polar solvents.<sup>54,65,75-77</sup> Moreover, the intensity ratio of  $S_{0-1}/S_{0-0}$  can be used to qualitatively evaluate the proximity of the PDI units in solution and the degree of aggregation in a given system.<sup>78</sup> This effect is further amplified by raising the aqueous concentration in the solvent, subsequently increasing the polarity of the medium and allowing for additional hydrogen bonding interactions. Raising the aqueous concentration up to 100% water results in a significant decrease in absorption in the visible region for copolymers **P3** and **P4** and the observable formation of micelles. This change can be attributed to the presence of an additional alkylated monomer, which significantly alters the polymer's hydrophobic properties. Interestingly, homopolymer **P2**, containing the highest content of PEG<sub>750</sub> chains, exhibits a clear absorption peak at 530 nm even with 100% water content. This can be rationalized as the effect of the PEG chains providing solubility in highly polar solvents, countering their aggregating impact on the PDI cores. When the solvent was replaced with a higher polarity



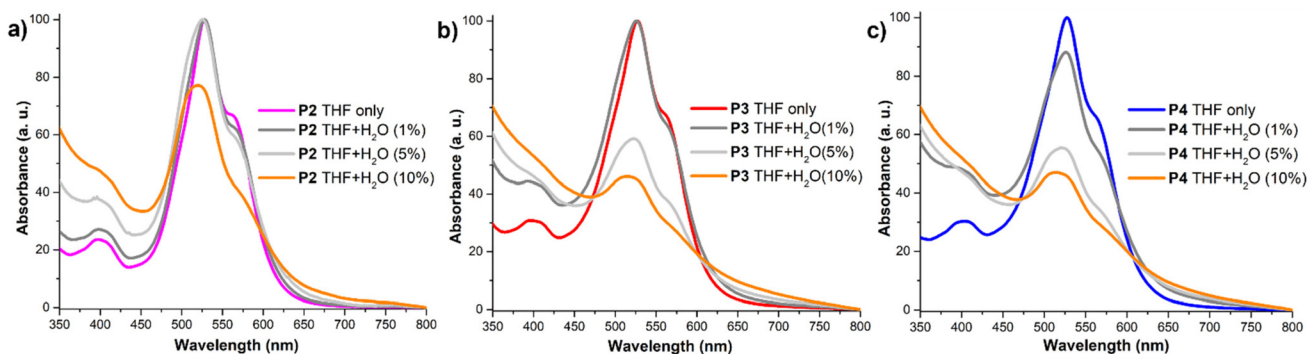


**Fig. 2** UV-Vis absorption spectra of (a) homopolymer **P2** in THF and combinations of THF and water, (b) diblock copolymer **P3** in THF and combinations of THF and water, and (c) triblock copolymer **P4** in THF and combinations of THF and water.

one such as methanol or a MeOH/water mixture copolymers **P3** and **P4** exhibited broad maxima around 530 nm with decreasing intensity as the water content increased. A similar trend was observed for **P2**; however, in solution the PDI absorption profile was retained, confirming the ability of **P2** to retain partial solubility in highly polar solvents (Fig. S14–S16, ESI†).

To further understand the aggregation modes of the polymers and their structure dependence, the emission spectra of polymers **P2**, **P3** and **P4** were analysed (Fig. 3). In a chloroform solution, the polymers exhibit an emission profile that closely matches the one reported in the literature for phenoxy *bay* functionalized PDI.<sup>66</sup> This spectrum shows strong peaks with a maximum at 593 nm and a characteristic shoulder in the emission spectrum at around 640 nm. In the thin film state, the emission spectra exhibit a singular strong band around the 700 nm region, which is consistent with previous reports on PDI-based aggregates and supramolecular structures.<sup>74,79–81</sup> Interestingly this emission is clearly visible in the solution of homopolymer **P2** and random copolymers **P3** and **P4**, which

can be assigned to enhanced  $\pi$ – $\pi$  interactions and the directing effect of the specific polymeric backbone structure (Fig. 3). In addition, analysis of the emission of the chloroform solutions and thin films of diblock polymers **P3** vs. **P5** (Fig. S17, ESI†) and triblock polymers **P4** vs. **P6** (Fig. S18, ESI†) indicated identical PDI-chromophore cores and degrees of aggregation, and thus the photophysical properties can be altered by changing the backbone composition. The films of polymers **P3**–**P6** exhibit consistent emission at 700 nm indicating that strong  $\pi$ – $\pi$  stacking is consistent with the 0–2 transition becoming predominant over the lower-energy processes in every scenario. Interestingly even in chloroform solution a significant emission band can be observed at 700 nm indicating that consistent distances between the PDI cores enforced by the polymer backbone support AEI, even in highly diluted media.

Due to their modular structure and amphiphilic properties, the polymers studied here exhibit solubility in a wide range of solvents and all three polymers display similar emissions in THF. However, the introduction of water results in significant and dramatic changes in their fluorescence profiles indicating different  $\pi$ – $\pi$  stacking aggregation of the PDI cores. Depending on the composition of the polymers and the solvent, the emissions from these polymers exhibit typical characteristic features of both solution and solid states. The homopolymer **P2** (Fig. 4a), which contains the highest concentration of both PEG<sub>750</sub> and PDI fragments, shows a significant decrease in emission at 586 nm when 5% water is added. However, when the aqueous concentration is increased up to 10%, there is only a minor further change in emission. This is accompanied by a red shift and a gradual enhancement of the 0–2 emission signal. This phenomenon can be estimated as reaching an equilibrium point where  $\pi$ – $\pi$  stacking interactions are balanced by the increasing impact of the PEG moieties in a more polar medium. In the case of the diblock polymer **P3** (Fig. 4b), which contains additional polar diester groups, there is a slower drop in the intensity of the main emission band at 587 nm upon the addition of water. However, there is a significant increase in the solid-state emission band when the aqueous concentration reaches up to 10%. We assume that the

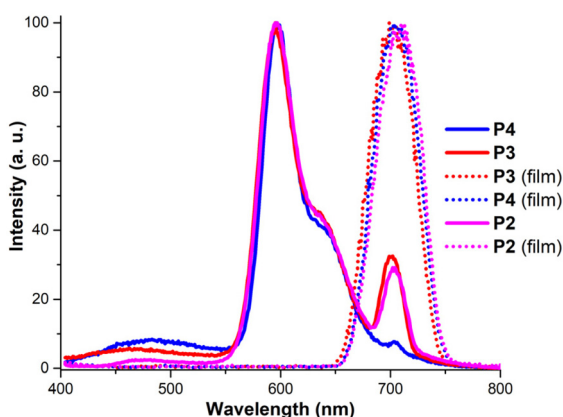


**Fig. 3** Emission spectra of homopolymer **P2** (pink solid line), diblock copolymer **P3** (red solid line) and triblock copolymer **P4** (blue solid line) in chloroform and the thin film state of **P3** (red dotted line), **P4** (blue dotted line) and **P2** (pink dotted line) cast from the same solvent.



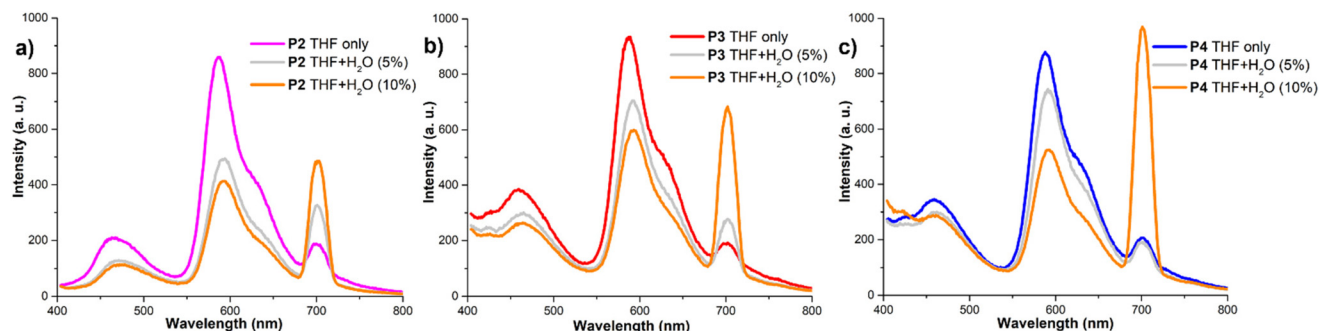
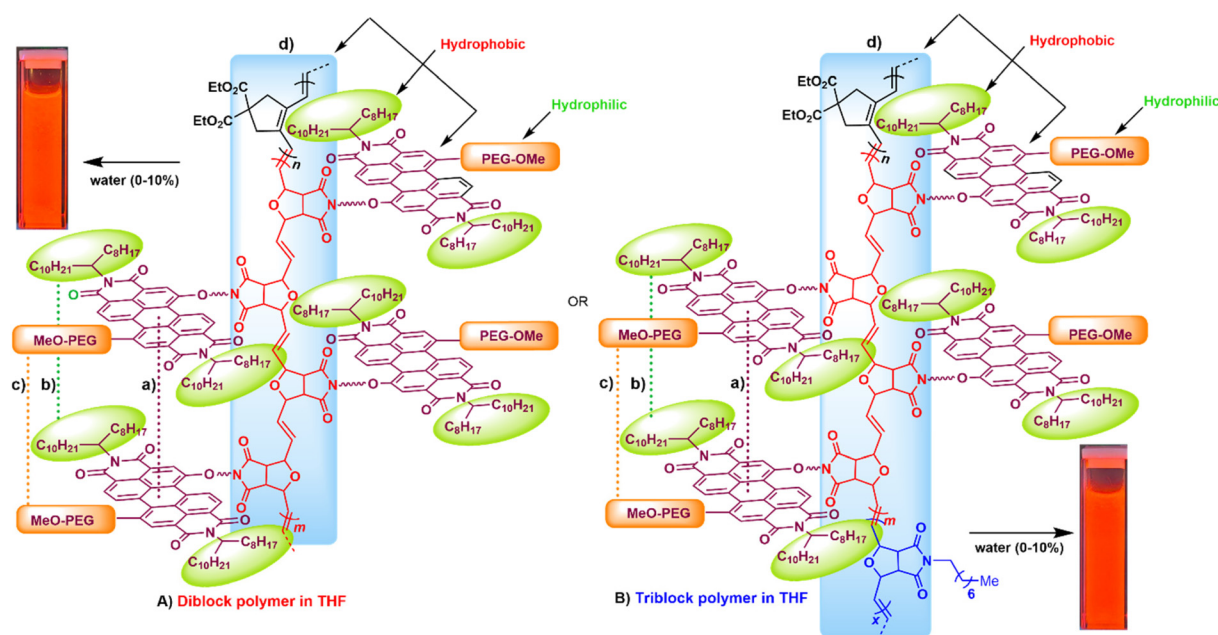


**Fig. 4** Emission spectra of (a) homopolymer **P2** in THF and combinations of THF and water, (b) diblock copolymer **P3** in THF and combinations of THF and water, and (c) triblock copolymer **P4** in THF and combinations of THF and water.

10% aqueous concentration in solution is the point at which the ester groups are no longer polar enough to keep the polymer in solution, leading to rapid aggregation. A similar scenario was observed for the triblock copolymer **P4** (Fig. 4c), where the presence of additional aliphatic fragments caused an even more pronounced increase in the solid-state emission at 700 nm, becoming the main band for this material. A schematic representation of the aggregation of both polymers **P3** and **P4** is outlined in Scheme 2 displaying self-assembling factors such as  $\pi$ -stacking and the formation of hydrophobic and hydrophilic domains as well as the directing effect of the backbone composition. When the solvent was replaced with the more polar MeOH the predominant peak at 700 nm was observed for all the polymers, with additional absorption at 600 nm observed for **P3** and **P4**. When the water content was increased from 0–100% all the polymers exhibited solely 700 nm maxima with various intensities (ESI†).

### Morphological properties of the block copolymers

To further confirm the copolymer sizes and self-assembly behaviors of **P3** and **P4**, their morphological properties were investigated using atomic force microscopy (AFM) and scanning electron microscopy (SEM) analysis. Samples for AFM and SEM analysis were prepared by casting drops of their chloroform solutions on a clean glass slide, followed by drying at room temperature. AFM was employed to investigate the morphology of solid films of the diblock copolymer **P3** (A) and triblock polymer **P4** (B) as shown in Fig. 5. The AFM images of polymers **P3** and **P4** clearly demonstrate the presence of globular and nano-ring like morphologies with clearly visible internal empty cavities between them. Similar morphological features have been reported and assigned to  $\pi$ - $\pi$  interactions between the PDI aromatic rings and H-bond driven aggregation.<sup>82</sup> As shown in Fig. 5, the AFM image of copolymer **P3** dis-



**Scheme 2** A schematic representation of aggregation of both polymers **P3** and **P4** displaying self-assembly factors such as (a)  $\pi$ -stacking, (b) and (c) formation of hydrophobic and hydrophilic domains and (d) the directing effect of backbone composition.





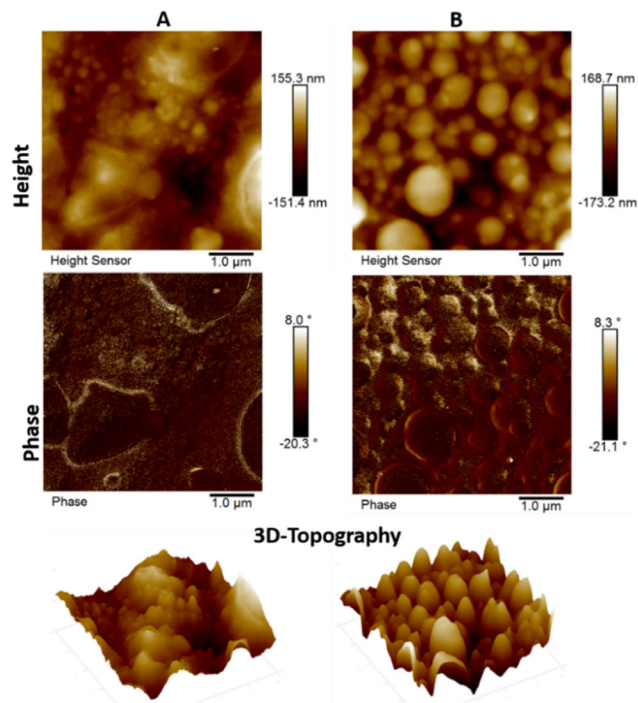


Fig. 5 AFM images and 3D-topographical plots of **P3** (A) and **P4** (B).

played a slightly more homogeneous texture in comparison to the triblock copolymer **P4**, which exhibited significant uniformity albeit with various globular deformations on the surface having spherical morphologies.<sup>82</sup> Furthermore, the AFM images show similar surface values of root-mean-square (RMS) roughness of 38.6 nm for **P3** and 40.6 nm for **P4**, which results in the grain size being comparable. These differences are indicated by the 3D-height topography presented on the same scale for both polymers. Similar thin film formations for both **P3** and **P4** were observed, which are smoother in general, but with some defects seen for **P3**, while **P4** is slightly rough but has smaller size irregularities on the order of nanometers in both cases.

Nearly spherical morphologies were also evidenced, as expected, by SEM analysis of the cross-sections of copolymers **P3** and **P4** confirming the surface morphologies determined by AFM analysis. SEM images of the copolymers also showed various sizes of spherical morphologies and aggregation of

cores dispersed within the poly(ene) and poly(oxanorbornene) copolymer matrix (Fig. 6A and B). It is well known that the dispersion of these polymer blocks in a polymer matrix plays a dominant role in influencing the morphological properties of the polymer.<sup>83</sup> However, the type of aggregation of PEG-grafted PDI groups and the phase separation in these two copolymers have not been well addressed by SEM analysis.<sup>84</sup>

## Conclusions

In summary, we successfully synthesized copolymers of highly conjugated poly(acetylene)s and PEG<sub>750</sub>-PDI-incorporating or *N*-alkyl-derived poly(olefin)s in a single polymer chain *via* one-pot tandem cyclopolymerization and ROMP methodologies. Both di- and tri-block copolymers and their random versions were prepared from 1,6-heptadiynes and oxanorbornene imide-based cycloolefin monomers using a trifluoroacetate-modified [Ru]-alkylidene-based metathesis initiator. The relative weight percentages of both di- and tri-block copolymers determined by XPS analysis revealed a slight excess of the percentages of atomic concentrations in the case of the triblock copolymers. The photophysical properties examined by UV-Vis and fluorescence spectroscopic analysis demonstrated different stages of the organization of the polymers in solution as well as in the formation of micelles upon diluting polymer solutions. Furthermore, these investigations provided more insight into the tuning and self-organization of PEG<sub>750</sub>-PDI derivatives of block copolymers in aqueous solution at various concentrations. In addition, AFM and SEM analysis elucidated copolymer surface and morphological information of both di- and tri-block polymers in their solid film state. In brief, our approach gives access to a variety of tunable PEG<sub>750</sub>-incorporating chromophores held by non-conjugated polymers as a copolymer counterpart of the cyclopolymerization-derived poly(acetylene). Based on our findings, tandem cyclopolymerization and subsequent ROMP-derived copolymers can be potentially used for the preparation of a variety of novel polymeric materials for electrical conductivity, bioimaging and photoluminescence applications.

## Author contributions

All authors have read and agreed to the published version of the manuscript.

## Conflicts of interest

There are no conflicts to declare.

## Acknowledgements

This work was supported by Texas A&M University at Qatar.

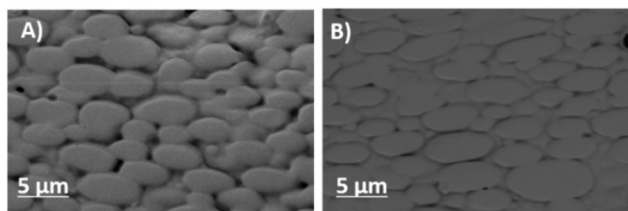


Fig. 6 SEM images of cross-sections of diblock copolymer **P3** (A) and triblock copolymer **P4** (B) films prepared by controlled evaporation from  $\text{CHCl}_3$ .





## References

- H. H. Fox and R. R. Schrock, *Organometallics*, 1992, **11**, 2763–2765.
- H. H. Fox, M. O. Wolf, R. O'Dell, B. L. Lin, R. R. Schrock and M. S. Wrighton, *J. Am. Chem. Soc.*, 1994, **116**, 2827–2843.
- F. J. Schattenmann and R. R. Schrock, *Macromolecules*, 1996, **29**, 8990–8991.
- P. S. Kumar, K. Wurst and M. R. Buchmeiser, *J. Am. Chem. Soc.*, 2009, **131**, 387–395.
- U. Anders, O. Nuyken, M. R. Buchmeiser and K. Wurst, *Angew. Chem., Int. Ed.*, 2002, **41**, 4044–4047.
- J. O. Krause, M. T. Zarka, U. Anders, R. Weberskirch, O. Nuyken and M. R. Buchmeiser, *Angew. Chem., Int. Ed.*, 2003, **42**, 5965–5969.
- S. K. Podiyanachari, H. S. Bazzi and M. Al-Hashimi, *Curr. Org. Chem.*, 2021, **25**, 2791–2805.
- E. B. Anderson, P. S. Kumar, D. Schawaller, S. Mavila, M. Voss, A. Freyer, W. Knolle, F. Hermanutz and M. R. Buchmeiser, *Macromol. Chem. Phys.*, 2013, **214**, 1047–1051.
- H. Li, J. Wang, H. Han, J. Wu and M. Xie, *React. Funct. Polym.*, 2018, **127**, 20–28.
- J. Wang, H. Li, X. Liao, M. Xie and R. Sun, *Polym. Chem.*, 2016, **7**, 4912–4923.
- M. R. Buchmeiser, *Polym. Rev.*, 2017, **57**, 15–30.
- K. Jung, E.-H. Kang, J.-H. Sohn and T.-L. Choi, *J. Am. Chem. Soc.*, 2016, **138**, 11227–11233.
- H. Jung, K. Jung, M. Hong, S. Kwon, K. Kim, S. H. Hong, T.-L. Choi and M.-H. Baik, *J. Am. Chem. Soc.*, 2018, **140**, 834–841.
- K. Jung, T. S. Ahmed, J. Lee, J.-C. Sung, H. Keum, R. H. Grubbs and T.-L. Choi, *Chem. Sci.*, 2019, **10**, 8955–8963.
- G. I. Peterson, S. Yang and T.-L. Choi, *Acc. Chem. Res.*, 2019, **52**, 994–1005.
- C. Kang, K. Jung, S. Ahn and T.-L. Choi, *J. Am. Chem. Soc.*, 2020, **142**, 17140–17146.
- E.-H. Kang and T.-L. Choi, *ACS Macro Lett.*, 2013, **2**, 780–784.
- E.-H. Kang, I. S. Lee and T.-L. Choi, *J. Am. Chem. Soc.*, 2011, **133**, 11904–11907.
- E.-H. Kang, S. Y. Yu, I. S. Lee, S. E. Park and T.-L. Choi, *J. Am. Chem. Soc.*, 2014, **136**, 10508–10514.
- C. Kang, E.-H. Kang and T.-L. Choi, *Macromolecules*, 2017, **50**, 3153–3163.
- S. Yang, S.-Y. Kang and T.-L. Choi, *J. Am. Chem. Soc.*, 2019, **141**, 19138–19143.
- K.-Y. Yoon, I.-H. Lee and T.-L. Choi, *RSC Adv.*, 2014, **4**, 49180–49185.
- E. H. Kang, S. Yang, S. Y. Yu, J. Kim and T. L. Choi, *J. Polym. Sci., Part A: Polym. Chem.*, 2017, **55**, 3058–3066.
- S. Yang, S.-Y. Kang and T.-L. Choi, *Nat. Commun.*, 2021, **12**, 2602.
- S. Yang and T.-L. Choi, *Chem. Sci.*, 2020, **11**, 8416–8424.
- S. Yang, S. Shin, I. Choi, J. Lee and T.-L. Choi, *J. Am. Chem. Soc.*, 2017, **139**, 3082–3088.
- H. Park, H.-K. Lee and T.-L. Choi, *Polym. Chem.*, 2013, **4**, 4676–4681.
- C. Kang, H. Park, J.-K. Lee and T.-L. Choi, *J. Am. Chem. Soc.*, 2017, **139**, 11309–11312.
- H. Park and T.-L. Choi, *J. Am. Chem. Soc.*, 2012, **134**, 7270–7273.
- J. Kim, E.-H. Kang and T.-L. Choi, *ACS Macro Lett.*, 2012, **1**, 1090–1093.
- S. K. Podiyanachari, S. Moncho, E. N. Brothers, S. Al-Meer, M. Al-Hashimi and H. S. Bazzi, *Macromolecules*, 2020, **53**, 4330–4337.
- M. Al-Hashimi, C. Hongfa, B. George, H. S. Bazzi and D. E. Bergbreiter, *J. Polym. Sci., Part A: Polym. Chem.*, 2012, **50**, 3954–3959.
- R. Tuba, R. Corrêa da Costa, H. S. Bazzi and J. A. Gladysz, *ACS Catal.*, 2012, **2**, 155–162.
- R. Tuba, M. Al-Hashimi, H. S. Bazzi and R. H. Grubbs, *Macromolecules*, 2014, **47**, 8190–8195.
- M. Al-Hashimi, M. A. Bakar, K. Elsaid, D. E. Bergbreiter and H. S. Bazzi, *RSC Adv.*, 2014, **4**, 43766–43771.
- M. Al-Hashimi, R. Tuba, H. S. Bazzi and R. H. Grubbs, *ChemCatChem*, 2016, **8**, 228–233.
- A. R. Hlil, J. Balogh, S. Moncho, H. L. Su, R. Tuba, E. N. Brothers, M. Al-Hashimi and H. S. Bazzi, *J. Polym. Sci., Part A: Polym. Chem.*, 2017, **55**, 3137–3145.
- R. Tuba, J. Balogh, A. Hlil, M. Barlóg, M. Al-Hashimi and H. Bazzi, *Engineering*, 2016, **4**, 6090–6094.
- J. Suriboot, C. E. Hobbs, W. Guzman, H. S. Bazzi and D. E. Bergbreiter, *Macromolecules*, 2015, **48**, 5511–5516.
- J. Suriboot, Y. Hu, T. J. Malinski, H. S. Bazzi and D. E. Bergbreiter, *ACS Omega*, 2016, **1**, 714–721.
- U. R. Gandra, A. Sinopoli, S. Moncho, M. NandaKumar, D. B. Ninković, S. D. Zaric, M. Sohail, S. Al-Meer, E. N. Brothers and N. A. Mazloum, *ACS Appl. Mater. Interfaces*, 2019, **11**, 34376–34384.
- U. R. Gandra, R. Courjaret, K. Machaca, M. Al-Hashimi and H. S. Bazzi, *Sci. Rep.*, 2020, **10**, 19519.
- S. K. Podiyanachari, M. Barlóg, M. Comí, S. Attar, S. Al-Meer, M. Al-Hashimi and H. S. Bazzi, *J. Polym. Sci.*, 2021, **59**, 3150–3160.
- M. Barlóg, S. K. Podiyanachari, S. Attar, D. N. Sredojević, H. S. Bazzi and M. Al-Hashimi, *Polym. Chem.*, 2022, **13**, 5912–5922.
- N. Jouault, Y. Xiang, E. Moulin, G. Fuks, N. Giuseppone and E. Buhler, *Phys. Chem. Chem. Phys.*, 2012, **14**, 5718–5728.
- E. Zhang, L. Liu, F. Lv and S. Wang, *ACS Omega*, 2018, **3**, 8691–8696.
- Z. Liang, R. A. Cormier, A. M. Nardes and B. A. Gregg, *Synth. Met.*, 2011, **161**, 1014–1021.
- K. Trofymchuk, A. Reisch, I. Shulov, Y. Mély and A. S. Klymchenko, *Nanoscale*, 2014, **6**, 12934–12942.
- X. Zhang, Z. Chen and F. Würthner, *J. Am. Chem. Soc.*, 2007, **129**, 4886–4887.



- 50 Z. Yang and X. Chen, *Acc. Chem. Res.*, 2019, **52**, 1245–1254.
- 51 E. Cohen, H. Weissman, I. Pinkas, E. Shimon, P. Rehak, P. Král and B. Rybtchinski, *ACS Nano*, 2018, **12**, 317–326.
- 52 H. Li and O. S. Wenger, *Angew. Chem., Int. Ed.*, 2022, **61**, e202110491.
- 53 P. Singh, A. Hirsch and S. Kumar, *TrAC, Trends Anal. Chem.*, 2021, **138**, 116237.
- 54 O. Krupka and P. Hudhomme, *Int. J. Mol. Sci.*, 2023, **24**, 6308.
- 55 L. Zong, H. Zhang, Y. Li, Y. Gong, D. Li, J. Wang, Z. Wang, Y. Xie, M. Han and Q. Peng, *ACS Nano*, 2018, **12**, 9532–9540.
- 56 Y. Hu, K. Wang, Y. Wang and L. Ma, *Dyes Pigm.*, 2023, **210**, 110948.
- 57 B. Zhang, I. Lyskov, L. J. Wilson, R. P. Sabatini, A. Manian, H. Soleimaninejad, J. M. White, T. A. Smith, G. Lakhwani and D. J. Jones, *J. Mater. Chem. C*, 2020, **8**, 8953–8961.
- 58 M. S. Ryoo, W. C. Lee and S. K. Choi, *Macromolecules*, 1990, **23**, 3029–3031.
- 59 S. K. Podiyanachari, M. Barlóg, M. Comi, S. Attar, S. Al-Meer, M. Al-Hashimi and H. S. Bazzi, *J. Polym. Sci.*, 2021, **59**, 3150–3160.
- 60 X. Wang, T. Zeng, M. Nourrein, B.-H. Lai, K. Shen, C.-L. Wang, B. Sun and M. Zhu, *RSC Adv.*, 2017, **7**, 26074–26081.
- 61 R. Chen, S. J. Benware, S. D. Cawthern, J. P. Cole, J. J. Lessard, I. M. Crawford-Eng, R. Saxena and E. B. Berda, *Eur. Polym. J.*, 2019, **112**, 206–213.
- 62 J. O. Krause, M. T. Zarka, U. Anders, R. Weberskirch, O. Nuyken and M. R. Buchmeiser, *Angew. Chem., Int. Ed.*, 2003, **42**, 5965–5969.
- 63 H. Park and T.-L. Choi, *J. Am. Chem. Soc.*, 2012, **134**, 7270–7273.
- 64 R. T. Mathers, K. Damodaran, M. G. Rendos and M. S. Lavrich, *Macromolecules*, 2009, **42**, 1512–1518.
- 65 F. Spreitler, M. Sommer, M. Thelakkat and J. Köhler, *Phys. Chem. Chem. Phys.*, 2012, **14**, 7971–7980.
- 66 Y. Chen, Y. Feng, J. Gao and M. Bouvet, *J. Colloid Interface Sci.*, 2012, **368**, 387–394.
- 67 W. S. Shin, H.-H. Jeong, M.-K. Kim, S.-H. Jin, M.-R. Kim, J.-K. Lee, J. W. Lee and Y.-S. Gal, *J. Mater. Chem.*, 2006, **16**, 384–390.
- 68 L. Rocard, A. Goujon and P. Hudhomme, *Molecules*, 2020, **25**, 1402.
- 69 E. E. Beauvilliers, M. R. Topka and P. H. Dinolfo, *RSC Adv.*, 2014, **4**, 32866–32875.
- 70 G. S. Perez, S. Dasgupta, W. Żuraw, R. F. Pineda, K. Wojciechowski, L. K. Jagadamma, I. Samuel and N. Robertson, *J. Mater. Chem. A*, 2022, **10**, 11046–11053.
- 71 Y. Zhang, X. Guo, W. Su, B. Guo, Z. Xu, M. Zhang and Y. Li, *Org. Electron.*, 2017, **41**, 49–55.
- 72 H. Chang, Z. Chen, X. Yang, Q. Yin, J. Zhang, L. Ying, X.-F. Jiang, B. Xu, F. Huang and Y. Cao, *Org. Electron.*, 2017, **45**, 227–233.
- 73 H. Liu, L. Shen, Z. Cao and X. Li, *Phys. Chem. Chem. Phys.*, 2014, **16**, 16399–16406.
- 74 J. Liu, Y. Zhang, C. Zhang, P. Zhang, R. Zeng, J. Cui and J. Chen, *Mater. Adv.*, 2020, **1**, 1330–1336.
- 75 C. Fuller and C. Finlayson, *Phys. Chem. Chem. Phys.*, 2017, **19**, 31781–31787.
- 76 P. Su, G. Ran, H. Wang, J. Yue, Q. Kong, Z. Bo and W. Zhang, *Molecules*, 2023, **28**, 3003.
- 77 Z. Chen, B. Fimmel and F. Würthner, *Org. Biomol. Chem.*, 2012, **10**, 5845–5855.
- 78 B. Fimmel, M. Son, Y. M. Sung, M. Grüne, B. Engels, D. Kim and F. Würthner, *Chem. – Eur. J.*, 2015, **21**, 615–630.
- 79 D. Sriramulu, E. L. Reed, M. Annamalai, T. V. Venkatesan and S. Valiyaveetil, *Sci. Rep.*, 2016, **6**, 35993.
- 80 J. Das, R. B. K. Siram, D. Cahen, B. Rybtchinski and G. Hodes, *J. Mater. Chem. A*, 2015, **3**, 20305–20312.
- 81 T. Tang, J. Qu, K. Müllen and S. E. Webber, *Langmuir*, 2006, **22**, 26–28.
- 82 P. Singh, P. Sharma, N. Sharma and S. Kaur, *J. Mater. Chem. B*, 2022, **10**, 107–119.
- 83 P. Chal, A. Shit and A. K. Nandi, *ChemistrySelect*, 2018, **3**, 3993–4003.
- 84 P. Moharana and G. Santosh, *Spectrochim. Acta, Part A*, 2023, **297**, 122696.

